

Physical conditions and element abundances in galaxies at redshift $0.001 < z < 3.4$: evolution trends

M. Contini

School of Physics and Astronomy, Tel Aviv University, Tel Aviv 69978, Israel

Accepted: Received ; in original form 2010 month day

ABSTRACT

We have collected an heterogeneous sample of galaxies at redshifts $0.001 \leq z \leq 3.35$ with the aim of exploring the evolution of the physical parameters and of the element abundances calculated by modelling the observed spectra. The evolution picture which results from our calculations shows that: 1) the emitting gaseous clouds in both active galactic nuclei (AGN) and starburst (SB) galaxies have a density broad peak at $z \sim 0.5$ becoming less dense and more elongated with time. 2) The $H\alpha$ flux emitted from the AGN clouds has a maximum at $z \sim 0.1$. 3) The observed star temperatures in SBs increase with time, indicating younger stars in local galaxies. 4) The O/H relative abundances show splitting between solar and ≥ 0.1 solar at $0.3 < z < 3$. N/H also shows splitting in this z range but it also has a broad flat maximum between $z = 0.1$ and $z = 0.001$. 5) The AGN narrow line region and the regions surrounding the SB show fragmentation at $z \geq 0.35$. 6) Metallicity (in terms of O/H) correlates with $H\alpha$ luminosity $L_{H\alpha}$ (and therefore with the star formation rate) with different trends regarding SBs and AGNs for $L_{H\alpha} \geq 10^{41}$ erg s $^{-1}$. A rough correlation is seen also for N/H. There seems to be no correlation for low luminosity galaxies.

Key words: radiation mechanisms: general — shock waves — ISM: abundances — galaxies: Seyfert — galaxies: starburst — galaxies: high redshift

1 INTRODUCTION

The evolution with redshift of galaxy physical characteristics and of the star formation rates (SFR) has been recently investigated in different types of galaxies (Teplitz et al. 2003, Caputi et al. 2007, Stierwalt et al 2013, Straughn et al. 2009, Shim et al. 2009, etc.).

The SFR is calculated from the $H\alpha$ luminosity ($L_{H\alpha}$) or from the infrared luminosity (L_{IR}), depending on the data available from the observations. $L_{H\alpha}$ therefore, together with the line intensities and profiles, gives us the information about the physical structure of the interstellar medium which is important to the formation of stars (Spaans & Carollo 1997). The mutual feedback of starbursts (SB) and active galactic nuclei (AGN) leads to an enhanced $H\alpha$ luminosity from the galaxy because both the SB and the AGN contribute. The $H\alpha$ emission line flux and the flux of lines corresponding to the other elements emitted from the gas close to the SB and from the gas ionized by the AGN radiation flux are summed up in the characteristic spectra observed at Earth (Contini 2013a).

Regarding the epoch of star forming activity, most stars in massive galaxies ($M > 10^{11} M_{\odot}$) formed ~ 8 -10 billion years ago, when star formation was at its maximum (Swin-

bank et al 2012). It is believed that the optimal metallicity (the metal production rate is a direct measure of the star formation rate) corresponds to a period of intense star formation at about $1 < z < 2$ (Spaans & Carollo 1997, Madau et al. 1996).

The abundances of the heavy elements in the surrounding of the starbursts are affected not only by the star activity at different ages, but also by galaxy interactions. The discovery of AGNs showing a double nucleus (e.g. Fried & Schultz 1983 for NGC 6240, Fabbiano et al 2011 for NGC 3393, etc) demonstrated that some local objects are the result of merging. Collision of galaxies at higher redshifts yields star formation by compressing, collisionally heating and ionizing the gaseous clouds throughout the galaxy. For instance, based on FIR data from the Herschel Space Observatory, Santini et al (2012) gave evidence of an enhanced star formation activity in the host galaxies of X-ray -selected AGN at $0.5 < z < 2.5$ as compared to non-active galaxies. X-rays may reveal high temperature gas downstream of high velocity shocks.

It is suggested that mergers and tidal interactions lead to a low O/H in the galaxy central region and that a high N/O could reveal a powerful starburst (Pustilnik et al. 2004). In a sample of star-forming luminous compact

arXiv:1310.5447v1 [astro-ph.CO] 21 Oct 2013

galaxies showing recent interactions at $z < 0.63$, Izotov et al. (2011) found significant scattering in N/O values, with probably enhanced nitrogen abundance (see also Contini et al 2012 regarding the local galaxy NGC 7212).

Metallicity is represented by the O/H relative abundance because oxygen is the most abundant of the heavy elements and the corresponding spectral lines are the strongest e.g. in the optical range. The N/O abundance ratio as a function of O/H is considered to be useful in determining the chemical evolution of galaxies (Edmunds & Pagel 1978; Torres-Peimbert et al. 1989; Vila Costas & Edmunds 1993; Izotov et al. 2006). Investigating the correlation between relative abundances and galaxy morphologies of blue compact galaxies at $0.20 \leq z \leq 0.35$, Chung et al (2013) found that the oxygen and nitrogen abundances may be related to the local environments of the galaxies.

Metallicity (in terms of O/H) is calculated from the [OIII]/H β and [OII]/H β line ratios. In an accompanying paper (Contini 2013b) we discuss the reliability of the results obtained by modelling spectra showing only a few oxygen to H β line ratios on the basis of the Kakazu et al (2007) ultraviolet emission line of extremely low metallicity galaxy sample at $z \sim 1$ and the Xia et al (2012) faint galaxy sample at $0.6 \leq z \leq 2.4$.

At low redshifts ($z \leq 0.1$) the calculated relative abundances are constrained by many lines from different elements in different ionization levels throughout UV-optical-infrared spectra, while the modelling of spectra at higher z is prevented when one or more key lines from both high and low ionization levels are leaking (see Contini 2013b). Therefore, at higher redshifts ($z > 0.1$) direct methods are generally adopted to determine O/H. The "direct" method (Kakazu et al. 2007, Isotov et al 2011), based on Seaton (1975) and Pagel et al (1992) works, requires three oxygen lines ([OIII]4959,5007, [OII]3727).

We use composite models accounting for the combined effect of photoionization from the AGN or from the SB and shocks (e.g. Contini 2013a and references therein) which are adapted to deal with the collisional processes throughout the mergers. Therefore, the choice of the models will be constrained by the FWHMs of the line profiles which give a hint about the velocity field.

The mutual interaction between the nuclear activity and the starbursts in the same object is investigated in this paper by two different kinds of models : those characterised by a power-law photoionising flux and those characterised by a black-body radiation flux. Both photoionization and shocks are accounted for in the calculation of the spectra.

The analysis of the spectra observed at different locations throughout the narrow emission line region (NLR) and beyond it in single AGN, allows to calculate the relative abundances of the heavy elements to H and the ages of processes, such as star formation in close or far regions from the AGN (Ishibashi et al 2013). The location of the collision zone is revealed by the shock velocity distribution throughout the galaxy (Contini et al 2012, Contini 2012a,b).

We have collected some samples of galaxy spectra at different redshifts $0.001 < z < 3.4$. The composed sample accounts for active and non-active galaxy samples and individual objects, including for instance X-ray selected AGN, ultraluminous infrared galaxies (ULIRGs), damped Ly α absorber (DLA) galaxies, Seyfert galaxies, 3CR radio galax-

ies, star-forming galaxies, low ionization nuclear emission regions (LINERs), SB galaxies, etc., observed with different angular and spectral resolutions. The galaxies were selected on the basis of their spectra, i.e. showing enough lines to yield a reliable modelling. Therefore, the composed sample is relatively poor in number of objects. Unfortunately, far away objects characterised by fragmented gaseous clouds with low densities and metallicities have been most probably excluded. Moreover, the observed line ratios which provide the tools for calculating the physical and chemical conditions in galaxies at each redshift, are often uncertain due to selection effects, calibration biases and different corrections from obscuration (Gunawardhana et al. 2013).

Samples of galaxies belonging to a certain class (e.g. active galaxies) and observed by similar techniques, generally cover restricted z ranges and show nearly the same lines for each object spectrum. In an accompanying paper (Contini 2013c, hereafter Paper I) we have investigated the sample of active galaxies observed by Ramos Almeida et al. (2013). The results of modelling show that the parameters exhibit some smooth or varying trends in the redshift range $0.4 < z < 1.15$. However, their interpretation is limited to a restricted although significant redshift range.

We believe that the results obtained by modelling the line spectra emitted from the gas within different types of galaxies will show the trends of the physical parameters such as e.g. density, shock velocity, star temperature, etc. and of the element abundances throughout the z range, independently from the object identity. Moreover, adopting an heterogeneous sample of galaxies, smooth profiles or well defined fluctuations throughout a relatively extended redshift range can be better recognised and interpreted in the light of galaxy evolution and age.

The samples gathered in this work are the following. At redshift ranges $1.1 \leq z \leq 3.35$ we have analysed the spectra observed by Brand et al. (2007) from optically faint ultraluminous IR galaxies (ULIRGs). The results of modelling Ramos Almeida et al. (2013) galaxy spectra covering the redshift range $0.4 < z < 1.15$, which were presented in Paper I, are accounted for. Recently, the spectrum of the damped Ly α absorber galaxy (DLA) in the $z=2.93$ QSO 2222-0964 has been presented by Krogager et al (2013). It has been added to our analysis. We included also the line spectrum observed by Schirmer et al (2013) from the galaxy J4022-0927 at $z=0.326$, because it covers the near UV- near IR range.

Our aim is also to find out and compare the physical conditions of galaxies at lower redshifts. The star-forming region spectra, e.g. the relic radio-galaxy at $z < 0.165$ presented by Capetti et al (2013) and the spectra observed in the HII regions of compact star forming galaxies at $0.11 < z < 0.5$ by Kobulnicky & Zarisky (1999, hereafter KZ99) are analysed.

To learn about the evolution of the characteristic parameters of active galaxies (both AGN and SB) on a large scale, we have extended the spectral sample to local galaxies, namely, AGNs and SBs, such as those included in the sample of the low ionization nuclear emission line regions (LINERs) by Contini (1997) and in the sample of starburst galaxies by Viegas et al (1999), as well as the local merger Seyfert galaxies (Contini 2012a,b, 2013a).

Our sample is not complete, so, in order to cover the

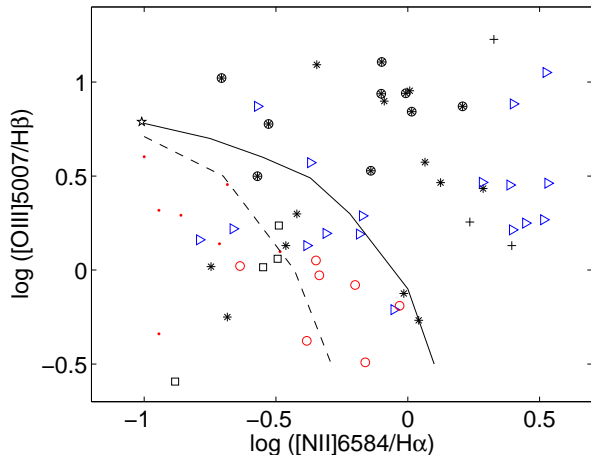


Figure 1. The distribution of the galaxies throughout a BPT diagram. Ramos Almeida et al. (2013): black asterisks; Brand et al (1997): black squares; Krogager et al (2013): black pentagram; KZ99: red dots; Winter et al (2010): black filled circles; Schirmer et al (2012): black asterisk; local mergers (Diaz et al 1988); Fosbury & Wall (1979); Veilleux et al. (1999) : black +; Capetti et al (2013): red circle; Contini (1997): blue triangles; Contini & Contini (2003) : red circles; the black dashed and solid lines represent the empirical separation between AGN and HII regions by Kewley et al (2001) and Kauffmann et al (2003), respectively

redshift range by a continuous distribution of the different parameters, we have included the data obtained from a subsample of galaxy spectra presented by Winter et al. (2010). We have selected the most observed objects and we have modelled the line ratios.

In Fig. 1 the line ratios observed from the selected galaxies are plotted throughout a Baldwin-Phillips-Terlevich (BPT) diagram (Baldwin et al. 1981). Fig. 1 shows that except for the HII region sample by KZ99 all the ensembles of line ratios within the other samples cross at least one of the lines separating AGNs from HII regions. The grids of calculated line ratios for local merger galaxies by Contini (2012a, fig. 1) show that the domains of AGN and SB in a BPT diagram may overlap.

The results of modelling the composed sample are presented in Sect. 2 and discussed in Sect. 3 in the light of evolution with z . Concluding remarks follow in Sect. 4.

2 MODELLING RESULTS

To calculate the spectra we have adopted the code SUMA¹, which simulates the physical conditions in an emitting gaseous cloud under the coupled effect of photoionization from an external radiation source and shocks (see Paper I for a detailed description of the code).

The input parameters which characterise the model are : the shock velocity V_s , the atomic preshock density n_0 , the preshock magnetic field B_0 . They define the hydrodynamical field and are used in the calculations of the Rankine-Hugoniot equations at the shock front and downstream.

¹ <http://wise-obs.tau.ac.il/~marcel/suma/index.htm>

These equations are combined into the compression equation which is resolved throughout each slab of the gas, in order to obtain the density profile downstream and consequently, the temperature of the gas. We adopt for all the models $B_0=10^{-4}$ gauss. The input parameter that represents the radiation field in AGNs is the power-law flux from the active centre F in number of photons $\text{cm}^{-2} \text{s}^{-1} \text{eV}^{-1}$ at the Lyman limit. The spectral indices are $\alpha_{UV}=-1.5$ and $\alpha_X=-0.7$. If the radiation flux is a black body radiation from the stars, the input parameters are the colour temperature of the star T_* and the ionization parameter U (in number of photons per number of electrons at the nebula).

The geometrical thickness of the emitting nebula D , the dust-to-gas ratio d/g , and the abundances of He, C, N, O, Ne, Mg, Si, S, A, and Fe relative to H are also accounted for.

In our models the flux from an external source can reach the shock front (the inflow case, indicated by the parameter $str=0$) or the edge of the cloud opposite to the shock front when the cloud propagates outwards from the AC or from the starburst (outflow, indicated by $str=1$).

The observed line ratios presented in the following are all reddening corrected.

2.1 Spectra from the Brand et al (2007) galaxy sample at $1.37 \leq z \leq 3.35$

In Table 1 we present the modelling of the spectra of optically faint ULIRGs at relatively high z reported by Brand et al. (2007). Their sample of 10 galaxies was selected from a 24 μm survey of the NOAO Deep Wide-Field Survey (NDWFS; Jannuzi & Dey 1999) Boötes field. The sample was observed by the NIRSPEC (McLean et al 1998) on the Keck II telescope or the NIRI (Hodapp et al 2003) on the Gemini North telescope.

We have reproduced the $[\text{NII}]6583/\text{H}\beta$ and $[\text{OIII}]5007/\text{H}\beta$ line ratios by models referring to AGNs (m_{AGN}) as well as by models referring to the starburst (m_{SB}). In the former case we have used both models showing clouds inflowing towards the AGN ($str=0$) and outflowing ($str=1$) from the galaxy. For starbursts, we consider that only the outflowing case makes sense. Most of the line observed fluxes are upper or lower limits. Moreover, the observed lines are not enough to distinguish between SB dominated or AGN dominated models. On the other hand, with the help of the FWHM of the forbidden lines, we could constrain the dynamical and therefore also the radiation parameters. We can thus obtain the distribution of the physical and chemical parameters at relatively high redshifts.

The observed line ratios in Table 1 are corrected for extinction adopting $E(B-V)$ values which appear in Brand et al (2007, table 1). The modelling results show that the photoionizing flux from the active centre does not exceed the values found for low ionization AGNs even at relatively high z . Perhaps this happens because Brand et al galaxies are ULIRGs and the high dust-to-gas ratio characteristic of ULIRGs (Contini & Contini 2002) can reduce the intensity of the flux reaching the clouds. Moreover the cloud geometrical thickness is low indicating strong fragmentation most probably due to turbulence related to the relatively high ve-

Table 1. Comparison of calculated with observed galaxies from the Brand et al (1997) sample at $1.37 \leq z \leq 3.3$

	z	[OIII]/H β	[NII]/H β	FWHM km s $^{-1}$	H β erg cm $^{-2}$ s $^{-1}$	V_s km s $^{-1}$	n_0 cm $^{-3}$	log F -	U -	T_* 10 4 K	N/H 10 $^{-5}$	O/H 10 $^{-4}$	D 10 15 cm	<i>str</i>
J ¹	1.37	0.34	0.38	375	<17.6 10 $^{-18}$	-	-	-	-	-	-	-	-	-
m_{AGN}	-	0.46	0.28	-	0.028	390	500	10	-	-	3.	2.6	2.2	0
m_{AGN}	-	0.5	0.5	-	0.02	390	500	10	-	-	3.	2.6	2.5	1
m_{SB}	-	0.32	0.3	-	0.018	390	300	-	0.01	3.	7.	3.	10	1
J ²	2.11	2.3	0.94	469	< 11.9 10 $^{-18}$	-	-	-	-	-	-	-	-	-
m_{AGN}	-	2.	0.93	-	0.013	450	300	10	-	-	3.5	6.6	1.3	0
m_{AGN}	-	2.23	1.	-	0.01	450	210	10	-	-	5.	6.6	1.3	1
m_{SB}	-	2.3	0.86	-	0.0038	480	320	-	0.002	4.	8.	6.	2.3	1
J ³	2.18	1.53	0.93	1617	<42.9 10 $^{-18}$	-	-	-	-	-	-	-	-	-
m_{AGN}	-	1.48	0.86	-	0.028	1600	210	10	-	-	9.	6.6	1.	0
m_{AGN}	-	1.44	0.8	-	5.7	1600	330	10	-	-	11.	7.6	1000.	1
m_{SB}	-	1.43	0.8	-	5.7	1600	330	-	0.01	3.	11.	7.6	1000.	1
J ⁴	2.223	1.38	0.82	585	<59.8 10 $^{-18}$	-	-	-	-	-	-	-	-	-
m_{AGN}	-	1.36	0.85	-	0.014	680	250	9.78	-	-	7.	6.	3.3	0
m_{AGN}	-	1.4	0.82	-	0.001	650	250	9.6	-	-	5.	6.	3.3	1
m_{SB}	-	1.45	0.72	-	0.007	600	250	-	0.004	2.	10.	5.	12.	1
J ⁵	3.355	1.87 ⁶	-	533	<57.9 10 $^{-18}$	-	-	-	-	-	-	-	-	-
m_{AGN}	-	1.65	0.6	-	0.009	550	250	9.6	-	-	10.	6.	3.3	0
m_{AGN}	-	1.44	0.85	-	0.0083	550	250	9.6	-	-	10.	6.	5.3	1
m_{SB}	-	1.45	0.72	-	0.007	600	250	-	0.004	2.	10.	5.	12.	1

¹ J143027.1+344007 ; ² J143011.3+343439 ; ³ J142842.9+342409 ; ⁴ J142800.7+350455 ; ⁵ J142644.3+333051 ;

⁶ not extinction corrected;

F is in photons cm $^{-2}$ s $^{-1}$ eV $^{-1}$ at the Lyman limit ;

Table 2. Comparison of calculated with observed line ratios to H β for the DLA galaxy (Krogager et al 2013) at $z=2.35$

	Ly α	[OII]	H β	[OIII]	H α	[NII]	H β erg cm $^{-2}$ s $^{-1}$	V_s km s $^{-1}$	n_0 cm $^{-3}$	log F -	U -	T_* 10 4 K	N/H 10 $^{-5}$	O/H 10 $^{-4}$	D 10 18 cm	<i>str</i>
obs	10.1	1.6	1	8.2	2.86	0.284	-	-	-	-	-	-	-	-	-	-
M_{AGN}	26.9	2.8	1	8.	2.9	0.4	0.21	130	400	10.8	-	-	2.	5.	1.	0
M_{SB}	26.7	1.8	1	8.24	2.9	0.48	0.075	130	450	-	0.09	4.5	7.	7.9	0.016	1

F is in photons cm $^{-2}$ s $^{-1}$ eV $^{-1}$ at the Lyman limit

locity shocks. In the case of SB, the temperature of the stars is rather low, as well as the ionization parameter.

2.2 The spectrum of the DLA galaxy at $z=2.35$ towards QSO, SDSSJ2222-0946

The emission line spectrum from the DLA galaxy at $z=2.35$ observed by Krogager et al. (2013) by VLT/X-shooter, shows the Ly α , [OII]3727+, [OIII]5007+, [NII]6584 besides H α and H β lines. The results of modelling the extinction corrected line ratios using both an AGN model and a SB model are shown in Table 2. The Ly α /H β line ratio is overestimated by a factor ≥ 2 by the models, however, lower values would lead to very low [OII]/H β , [OIII]/H β and [NII]/H β . This indicates that many different conditions contribute to the observed spectrum. We derived O/H = 5 10 $^{-4}$ and 7.9 10 $^{-4}$, (while Krogager et al. 2013 found O/H=2.5 10 $^{-4}$) and N/H = 2 10 $^{-5}$ and 7 10 $^{-5}$ for AGN and SB models, respectively,

The shock velocities deduced from the FWHM of the line profiles are rather low ($V_s \sim 130$ km s $^{-1}$) and the preshock densities ($n_0 \sim 400$ cm $^{-3}$) are consistent with those found for other Ramos Almeida et al objects in Paper I.

2.3 The line spectrum of the Seyfert galaxy J2240-0927 at $z=0.326$

We would like to include to the analysis of the physical conditions in galaxies at $z \leq 0.5$ the spectrum of one of the "Green Been" prototype galaxies observed by Schirmer et al (2012), J2240-0927 at $z=0.326$, which shows one of the most luminous NLR of Seyfert 2 galaxies. Characteristic of this galaxy is the extended NLR covering more than 26×44 kpc 2 and the large region surrounding the NLR. The spectrum is based on observations made with the ESO Telescopes at La Silla and Paranal Observatories in Chile, and observations obtained with MegaPrime/MegaCam and by the Gemini Observatory.

The ratios of selected emission lines (corrected for extinction) to H β are reported in Table 3. Schirmer et al suggest velocities between 200 and 300 km s $^{-1}$ calculated from the FWHM of the line profiles. We will constrain the models adopting this velocity range. The spectrum is rich of lines from the near UV - optical- near IR ranges. The [NeIII]/H β line ratio is overpredicted by the models accounting for the summed $\lambda 3689$ and $\lambda 3956$ line components. However, a high [NeV]/H β cannot be obtained by models MJ₂₀₀ and MJ₆₀₀ which show a satisfactory agreement for all the

Table 3. Comparison of calculated with observed line ratios for the galaxy J2240-0927 at $z=0.326$

line	obs	MJ ₂₀₀	MJ ₆₀₀	MJ _{IF}	MJ _{IFIV}
MgII 2789	0.24	0.3	0.34	0.4	0.18
[NeV] 3427	0.22	0.06	0.06	0.2	0.13
[OII] 3727+	3.72	4.4	2.6	3.	3.9
[NeIII] 3869+	0.71	1.0	1.2	0.96	1.2
H γ	0.40	0.46	0.46	0.46	0.46
[OIII] 4363	0.13	0.07	0.08	0.05	0.09
HeII 4686	0.13	0.27	0.27	0.15	0.27
H β	1	1	1	1	1
[OIII] 5007+	10.56	9.8	10.9	1.84	9.83
HeI 5876	0.09	0.12	0.12	0.18	0.11
[OI] 6300+	0.55	0.3	0.4	1.65	0.13 ¹
H α	4.25	2.9	2.9	3.	2.9
[NII] 6584+	2.36	2.9	2.7	3.9	2.9
[SII] 7617+	2.11	1.5	0.7	1.3	0.75
[ArIII] 7138+	0.11	0.14	0.15	0.1	0.16
[SIII]9071+	1.71	2.07	2.4	2.1	1.5
HeI 10833	0.30	0.65	0.96	1.09	0.6
<hr/>					
H β abs ²	-	0.057	0.173	0.05	0.03
V _s (km s ⁻¹)	-	200.	600.	600.	300.
n ₀ (cm ⁻³)	-	390.	360.	360.	280.
<i>F</i> (10 ¹⁰ units ³)	-	3.	9.	2.	2.
<i>D</i> (10 ¹⁵ cm)	-	6.	6.	6.	6.
<i>n</i> (10 ³ cm ⁻³)	-	10	28.	28.	9.3
N/H (10 ⁻⁵)	-	7.	7.	7.	7.
O/H (10 ⁻⁴)	-	6.6	6.6	6.6	6.6
Ne/H (10 ⁻⁴)	-	1.	1.	1.	1.2
Mg/H (10 ⁻⁶)	-	5.	5.	5.	5.
S/H (10 ⁻⁵)	-	1.6	1.6	1.6	2.
Ar/H (10 ⁻⁶)	-	1.3	1.3	1.3	1.3
str	-	1	1	1	1

¹ +[SIII]6312; ² H β calculated absolute flux in erg cm⁻² s⁻¹; ³ in photons cm⁻² s⁻¹ eV⁻¹ at the Lyman limit

other lines. A lower flux must be adopted. In the case of a model corresponding to $V_s = 600$ km s⁻¹, a lower F reduces too much the [OIII]5007+/[OI]6300+ line ratio. A better fit to the [NeV]/[NeIII] results adopting both a low flux and a low V_s . The models which refer to the outward motion of the NLR clouds better explain the observed line ratios than those referring to inflow.

We have found that N/H (7. 10⁻⁵) is slightly lower than solar (10⁻⁴), O/H and Ne/H are solar and Mg/H= 6.10⁻⁶ while the solar value is 2.6 10⁻⁵.

2.4 Relic radiogalaxies ($z \leq 0.3$)

Capetti et al (2013) presented the optical spectra of 3CR radiogalaxies at $z < 0.3$. which they interpreted as relic AGNs. The only object of the sample which shows data suitable to modelling is 3C 258. The line ratios are characteristic of star-forming regions, therefore we have modelled the spectrum by a starburst model. The results appear in Table 4. Capetti et al claim that the object is very compact for its redshift and the arc-like structure at SE suggests a recent merger. O/H is about solar and N/H is 0.3 solar.

Table 4. Comparison of calculated with observed line ratios for 3C 258 at $z=0.165$

	obs	model
H β	1.	1.
[OIII] 5007+	1.4	1.45
[OI] 6300+	0.27	0.2
[NII] 6548+	0.67	0.6
[SII] 6717	0.87	0.73
[SII] 6731	0.53	0.7
V _s (km s ⁻¹)	-	300
n ₀ (cm ⁻³)	-	40
T* (10 ⁴ K)	-	4.7
<i>U</i>	-	0.02
<i>D</i> (10 ¹⁹ cm)	-	1.
N/H (10 ⁻⁵)	-	3.
O/H (10 ⁻⁴)	-	7.
S/H (10 ⁻⁵)	-	1.
H β (erg cm ⁻² s ⁻¹)	-	0.0054
<i>n</i> (cm ⁻³)	-	506.

2.5 Star-forming galaxies and compact narrow emission-line galaxies ($0.11 < z < 0.5$)

The spectra of HII regions in 14 star-forming emission-line galaxies (ELGs) at $0.11 < z < 0.5$ were reported by Kobulnicky & Zaritsky (1999, hereafter KZ99), in order to investigate, in particular, the N/H and O/H relative abundances. The spectra were obtained by the Keck II telescope and low-resolution imaging multiobject spectrograph. The emission line widths of the observed galaxy sample are smaller than those of the local ones. Moreover KZ99 claim that these galaxies are slightly more metal-deficient and that metallicity of a galaxy increases monotonically with age.

We have modelled these spectra by SB models as we have done for previous galaxies. The results are presented in Tables 5, 6 and 7. We have found, by a detailed modelling, lower than solar relative abundances for N/H, O/H and Ne/H, by factors ≤ 10 , between ~ 1 and 4 and ≤ 3 , respectively. S/H shows lower than solar values even in local galaxies because S can be easily trapped into dust grains. KZ99 have found by direct O/H measurements that O/H ranges from a minimum of 10⁻⁵ for SA 68-206985 to a maximum of 1.9 10⁻⁴ for SDG 223, which are lower than solar by factors of 66 and 3.5, respectively. They found lower N/O relative abundances by a factor ~ 10 . The values obtained by the KZ99 empirical method are higher.

Table 4 shows that compared with the KZ99 sample of star forming galaxies, Capetti et al. 3C 258 relic galaxy corresponds to a shock velocity about double and a similar preshock density. The star temperature is slightly higher and the ionization parameter is similarly low, as well as the N/H and S/H relative abundances. On the other hand, O/H is about solar.

2.6 LINERs and SB galaxies at $z \leq 0.03$

So far the distribution of the AGNs at low z along the redshift axis for both AGN and SB is rather poor. Therefore, we have inserted in our sample the physical parameters which were calculated for other galaxies in previous works, e.g. for LINERs from the sample (Table 8) presented by Con-

Table 5. Comparison of calculated with observed line ratios to $H\beta$ for the KZ99 sample

galaxy	[OII] 3727+	[NeIII] 3869+	$H\gamma$ 6340	[OIII] 4363	HeI 4471	HeII 4686	[OIII] 5007+	HeI 5876	[SIII] 6312+	$H\alpha$ 6564	[NII] 6584+	[SII] 6717	[SII] 6731	z
L2-408115	3.8	<0.1	0.43	<0.025	<0.03	<0.024	1.67	0.12	<0.020	2.92	0.95	0.6	0.45	0.197
cal1	4.2	0.13	0.46	0.03	0.05	0.0002	1.55	0.055	2.96	0.978	0.637	0.47		
L2-410083	0.6	0.51	0.48	0.15	0.038	<0.008	8.88	0.106	<0.005	2.86	0.024	0.064	0.051	0.109
cal2	0.60	0.46	0.46	0.04	0.046	0.38	8.1	0.1	0.007	2.9	0.028	0.04	0.04	
L2-411500	3.38	0.36	0.46	0.031	<0.1	0.012	4.485	0.09	<0.06	-	-	-	-	0.193
cal3	4.1	0.39	0.46	0.06	0.09	0.00063	4.6	0.13	0.068	2.9	1.1	0.25	0.23	
SA 68 ^a	1.93	0.127	0.44	<0.012	<0.011	<0.011	2.77	0.07	<0.023	2.87	<0.33	0.406	0.386	0.285
cal4	2.5	0.2	0.46	0.03	0.048	0.0003	2.84	0.13	0.1	3.	0.38	0.37	0.38	
SDG 125	3.67	0.27	0.46	<0.014	0.036	<0.01	3.14	0.13	<0.003	-	-	-	-	0.3989
cal5	3.8	0.21	0.46	0.046	0.047	0.0003	3.66	0.136	0.035	3.	0.46	0.14	0.15	
SDG 146	1.94	<0.07	<0.36	<0.051	<0.26	<0.025	1.48	<0.1	<0.28	-	-	-	-	0.4006
cal6	2.2	0.12	0.46	0.019	0.047	0.00028	1.58	0.14	0.02	3.	0.38	0.11	0.13	
SDG 173A	3.4	<0.1	0.484	<0.065	<0.1	<0.09	3.8	<0.17	<0.4	<0.39	<0.6	<0.16	<0.16	0.3996
cal7	3.8	0.21	0.46	0.046	0.047	0.0003	3.66	0.136	0.035	3.	0.46	0.14	0.15	

^a SA 68-206134**Table 6.** Comparison of calculated with observed line ratios to $H\beta$ for the KZ99 sample

object	[OII] 3727+	[NeIII] 3869+	$H\gamma$ 6340	[OIII] 4363	HeI 4471	HeII 4686	[OIII] 5007+	HeI 5876	[SIII] 6312+	$H\alpha$ 6564	[NII] 6584+	[SII] 6717	[SII] 6731	z
SDG 183	3.	<0.06	0.411	<0.033	<0.037	<0.036	2.61	<0.043	<0.46	2.48	<0.4	<0.03	<0.03	0.3994
cal8	3.5	0.09	0.46	0.03	0.04	5.e-4	2.74	0.13	0.01	3.	0.44	0.04	0.04	
SDG 223	1.78	0.243	0.46	0.027	0.035	<0.01	5.34	0.12	<0.04	2.9	0.29	<0.09	<0.09	0.3996
cal9	1.4	0.25	0.46	0.012	0.05	0.02	5.3	0.15	6.e-5	2.95	0.34	0.08	0.08	
SDG 231	3.53	<0.15	0.44	<0.015	<0.014	<0.045	0.61	<0.06	<0.189	2.86	<0.33	<0.16	<0.16	0.3989
cal10	3.2	0.11	0.45	0.04	0.08	0.002	0.63	0.26	4.e-4	3.1	0.28	0.16	0.16	
L2-408570	3.4	<0.144	<0.304	<0.12	<0.09	<0.09	2.05	-	-	-	-	-	-	0.496
cal11	4.	0.16	0.43	0.15	0.15	0.004	1.9	0.5	3.e-3	3.56	0.1	0.05	0.04	
L2-408939	3.03	<0.009	0.47	0.078	<0.07	<0.06	3.55	<0.27	<0.058	-	-	-	-	0.425
cal12	2.3	0.06	0.46	0.02	0.05	0.002	3.7	0.15	0.002	2.94	0.12	0.03	0.024	
SA 68 ^a	2.	<0.05	<0.316	<0.095	<0.07	<0.06	0.85	<0.93	<0.208	-	-	-	-	0.4311
cal13	2.2	0.046	0.46	0.015	0.06	0.002	0.91	0.19	4.e-4	2.99	0.28	0.2	0.2	
SA 68 ^b	2.54	<0.09	0.727	<0.084	<0.08	<0.077	1.84	<0.12	<0.133	2.09	<0.56	0.83	0.755	0.2343
cal14	2.4	0.05	0.46	0.013	0.06	0.0013	1.81	0.17	0.001	2.98	0.48	0.67	0.73	

^a SA 68-206895; ^b SA 68-207213**Table 7.** The physical parameters and relative abundances for the models presented in Tables 5 and 6 for the KZ99 sample

model	V_s km s ⁻¹	n_0 cm ⁻³	T_* 10 ⁴ K	U -	D 10 ¹⁷ cm	N/H 10 ⁻⁴	O/H 10 ⁻⁴	Ne/H 10 ⁻⁴	S/H 10 ⁻⁵	$H\beta$ abs erg cm ⁻² s ⁻¹	n_H cm ⁻³	z
cal1	50	60	4.	0.0026	18.8	0.3	3.	0.5	2.1	0.0009	90.	0.197
cal2	130	80	4.8	22	9.5	0.1	5.6	0.7	0.8	0.056	590	0.109
cal3	70	90	4.3	0.014	8.	0.3	1.8	0.3	1.	0.0046	283	0.193
cal4	70	160	4.2	0.018	2.4	0.15	2.	0.3	2.5	0.014	626	0.285
cal5	70	170	4.2	0.018	2.67	0.15	2.5	0.3	0.8	0.015	692	0.3989
cal6	80	190	4.2	0.018	1.98	0.15	2.	0.3	0.8	0.025	1000	0.4006
cal7	70	170	4.2	0.018	2.7	0.15	2.5	0.3	0.8	0.015	690	0.3996
cal8	80	160	4.3	0.016	1.8	0.1	1.5	0.1	0.15	0.012	800	0.3994
cal9	120	90	5.5	0.2	8.	0.4	6.5	0.7	0.1	0.024	648	0.3996
cal10	120	90	4.9	0.002	8.	0.1	4.5	0.7	0.2	0.0023	647	0.3989
cal11	110	90	4.	0.0001	8.	0.1	4.	0.4	0.2	0.00054	585	0.496
cal12	60	50	4.4	0.015	8.	0.1	4.5	0.2	0.1	0.0019	119	0.425
cal13	120	90	4.9	0.008	8.	0.1	3.	0.2	0.2	0.0058	643	0.4311
cal14	130	90	4.5	0.025	8.	0.3	6.6	0.4	1.	0.012	700	0.2343

Table 8. The sample of LINERs by Contini (1997)

galaxy	z										
NGC 315	0.0165	NGC 404	0.0182	NGC 1052	0.0005	NGC 1167	0.0165	NGC 1275	0.0175	NGC 1667	0.0139
NGC 2639	0.011	NGC 2841	0.0024	NGC 3031	0.0001	NGC 3504	0.0005	NGC 3642	0.0053	NGC 3998	0.0035
NGC 4395	0.001	NGC 4618	0.002	NGC 7217	0.0031	NGC 7479	0.008	NGC 7714	0.0094	NGC 7743	0.0056

Table 9. The sample of SB galaxies by Viegas et al. (1999)

galaxy	z	galaxy	z	galaxy	z	galaxy	z
II Zw 40	0.0027	NGC 5253	0.0014	NGC 3690	0.01	NGC 3256	0.0093
M82	0.008	M83	0.00165	NGC 253	0.0158	NGC 4945	0.0019

tini (1997) based on the observations of Ho et al. (1993). Moreover, we have added the results from the sample of SB galaxies (Table 9) presented by Viegas et al (1999). In Tables 8 and 9 the galaxy names are followed by their redshift.

Still, we could not cover the whole range of z between 0.001 and 0.11 uniformly.

2.7 AGN spectra from the Winter et al. (2010) local galaxy sample

We collected the spectra of galaxies at the redshifts where the calculated data were missing, selecting a subsample of AGNs from the *SWIFT* Burst Alert Telescope survey, that was reported by Winter et al. (2010). Spectra including lines such as $H\alpha$, $H\beta$, [OIII] 5007+, [OI] 6300+, [NII] 6584+, [SII] 6717+ are suitable to a reliable modelling. We present the results of modelling in Tables 10, 11 and 12. Some of the selected galaxies, e.g. NGC 4151, were observed and modelled previously in different locations throughout the galaxy (Contini, Viegas, Prieto 2002 and references therein). We chose Winter et al data because referring to averaged spectra. As we have done for the Ramos Almeida et al (2013) sample in Paper I, we selected some objects whose spectra could be satisfactorily modelled also by starburst models showing the eventual contribution of starbursts to the AGN. In Table 10 the observed corrected data for each galaxy are followed by the model results in the next rows. Models m1-m10 refer to the AGN and the results are reported in Table 11. Models m4sb, m5sb and m8sb refer to the SB and are reported in Table 12. For all the models $Ne/H = 10^{-4}$ is adopted.

3 EVOLUTION OF THE PHYSICAL PARAMETERS AND OF THE RELATIVE ABUNDANCES

We assume as *results* of our analysis the input parameter set which leads to the best fit of the line ratios (and of the continuum SED, when observed) for each single object. The modelling precision is shown in Fig. 2 where the calculated and observed [OIII]5007+/ $H\beta$ and [NII] 6548+/ $H\beta$ line ratios are compared (left and right diagram, respectively). For the samples containing one only galaxy the approximation of model results to the data can be easily estimated from

the tables, therefore they are omitted in Fig. 2. The observed [OIII]5007+/ $H\beta$ for Ramos Almeida et al. (2013) galaxy G107 is an upper limit, therefore Fig. 2 shows that this line ratio is not exactly reproduced by the model. The comparison of [NII]/ $H\beta$ line ratios in Fig. 2 right diagram shows some scattering. In fact the observed [NII] lines can be affected by blending with $H\alpha$. Fig. 2 shows that Ramos Almeida et al. (2013) G60 galaxy is more likely AGN dominated.

The trends of the physical parameters and of the relative abundances calculated by modelling AGN and SB spectra of galaxies at redshifts $0.001 \leq z \leq 3.35$ are presented in Fig. 3. Besides V_s , n_0 , F , U , T_* , D and the relative abundances, we draw special attention to the $H\alpha$ absolute flux $H\alpha_{calc}$, calculated for the single objects, and to the geometrical thickness D of the emitting clouds which cannot be predicted directly from the line ratios but only from model calculations. They are connected with the luminosity of the galaxies and with the emitting cloud dimensions, respectively. $L_{H\alpha}$ measured at Earth is related with the $H\alpha$ flux emitted by the nebulae (the NLR for AGNs and the region surrounding the SB) throughout the galaxy and with the radius of the NLR and SB regions R : $L_{H\alpha}(\text{Earth}) = H\alpha(\text{Earth}) \times 4\pi d^2 = H\alpha_{calc}(\text{nebula}) \times 4\pi R^2$, where d is the distance to Earth.

3.1 Parameters referring to the shock

Fig. 3 top left panel refers to n_0 and V_s . Preshock densities in the emitting clouds range between ~ 50 and $> 1300 \text{ cm}^{-3}$. Recall that the density in the downstream region of the clouds, where both the line and continuum spectra are emitted, is higher than n_0 by a factor of 4 to >100 , depending on the shock velocity.

We have found that galaxies at $0.4 \leq z \leq 3$ show relatively high preshock densities ($500\text{-}1300 \text{ cm}^{-3}$) which may indicate that the gas has been compressed by shock waves created by collision during galaxy merging.

The density increases with decreasing z from $z=3.35$ to $z=0.5$ which corresponds to the top of a broad n_0 peak. Then, n_0 decreases towards $z=0.1$. At low z , n_0 regains values between ~ 100 and 600 cm^{-3} , the highest for SB galaxies.

Shock velocities were derived as a first choice from the FWHM of line profiles of each object referring to the NLR or to the SB surrounding clouds. Then they were slightly

Table 10. Comparison of calculated with observed line ratios to H β for the Winter et al (2010) sample

galaxy	FWHM ¹	[OIII]5007+	[OI]6300+	[NII]6548+	[SII]6717+	z
NGC 3516	582	9.28	0.345	3.0	1.2	0.009
m1	-	8.9	0.34	3.1	1.62	-
3C 105	240	17.07	0.33	2.31	1.17	0.089
m2	-	17.12	0.446	2.88	0.8	-
3C 111	214	14.01	0.3	0.57	0.81	0.049
m3	-	14.5	0.33	0.74	0.82	-
Mrk 110	483	7.98	0.49	0.86	0.7	0.035
m4	-	8.43	0.24	1.	0.74	-
m4sb	-	8.6	0.23	0.64	0.9	-
Mrk 1498	320	4.21	0.15	0.78	0.75	0.055
m5	-	4.4	0.144	0.86	0.79	-
m5sb	-	4.1	0.2	0.85	0.86	-
3C 403	270	11.62	0.48	2.85	1.77	0.059
m6	-	12.3	0.5	2.6	1.2	-
Mrk 1018	693	9.91	0.33	4.68	2.08	0.043
m7	-	10.	0.3	4.2	1.0	-
Mrk 813	1486	4.74	0.21	-	1.50	0.11
m8	-	4.8	0.23	1.12	1.	-
m8sb	-	4.49	0.16	0.37	0.9	-
NGC 4051	227	4.5	0.46	2.1	1.19	0.002
m9	-	4.4	0.4	2.6	1.0	-
NGC 4151	488	11.56	0.75	2.3	1.84	0.003
m10	-	11.	0.9	2.8	1.2	-

¹ in km s⁻¹**Table 11.** The physical conditions for the AGN models in the Winter et al (2010) sample

	z	V _s km s ⁻¹	n ₀ cm ⁻³	F units ¹	N/H 10 ⁻⁵	O/H 10 ⁻⁴	S/H 10 ⁻⁵	D 10 ¹⁷ cm	H β abs units ²
NGC 3516	0.009	550	40	0.5	10.	6.6	1.8	3.6	0.019
3C 105	0.089	200	250	10.	7.	6.6	1.8	1.19	0.185
3C 111	0.049	200	250	8.	2.	6.6	1.8	1.1	0.18
Mrk 110	0.035	400	50	0.9	5.	6.6	1.5	75.	0.043
Mrk 1498	0.055	320	400	1.	2.	5.6	2.5	0.029	0.15
3C 403	0.059	200	250	8.	7.	5.6	2.2	15.4	0.3
Mrk 1018	0.043	700	350	0.7	10.	6.6	2.9	0.042	0.005
Mrk 813	0.11	1400	70	0.8	2.	4.6	1.5	0.123	0.02
NGC 4051	0.002	250	230	0.8	5.	6.6	1.5	0.096	0.012
NGC 4151	0.003	500	40	0.4	7.	6.6	1.5	14.	0.012

¹ in 10¹⁰ photons cm⁻² s⁻¹ eV⁻¹ at the Lyman limit; ² in erg cm⁻² s⁻¹**Table 12.** The physical conditions for the SB models in the Winter et al (2010) sample

	z	V _s km s ⁻¹	n ₀ cm ⁻³	T _* 10 ⁴ K	U -	N/H 10 ⁻⁵	O/H 10 ⁻⁴	S/H 10 ⁻⁵	D 10 ¹⁷ cm	H β abs units ¹
Mrk 110	0.035	400	50	7.	1.	5.	6.6	0.5	20.	0.044
Mrk 1498	0.055	320	400	6.	0.1	4.	6.6	1.3	10.	0.23
Mrk 813	0.11	1400	100	6.5	1.	2.	4.6	1.5	10.	0.26

¹ in erg cm⁻² s⁻¹

modified cross-checking the modelling of the line ratios. V_s ranges between 100 and 1600 km s⁻¹, with an increasing trend with z from z=0.6 to z=3.35. The opposite trends of V_s and n₀ in the same z range are in agreement with the Rankine-Hugoniot law of conservation of matter throughout the shock front and downstream. This suggests that the dynamical parameters, e.g. V_s and n₀ at relatively low z, are most probably connected with phenomena on small scales

in regions within the galaxy, rather than with evolution of galaxies on a Hubble time scale.

The shock velocities deduced from modelling are in the same range for AGN at high and low z. The lowest V_s appear for the HII star forming regions of compact galaxies (KZ99).

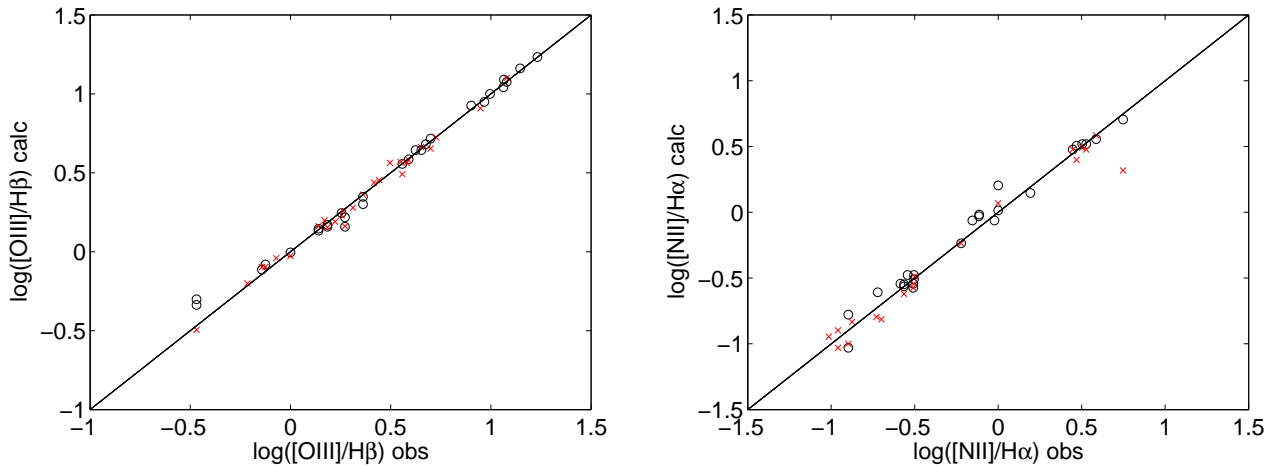


Figure 2. Comparison between calculated and observed line ratios for the galaxies. Models for AGN : black circles; SB models : red crosses; the solid line is the 1:1 line.

3.2 The photoionising radiation flux

Fig. 3 top right panel shows the trend of the temperature of the stars T_* (in units of 10^4 K) in SB galaxies, in the SBs included in the LINER sample and in samples at higher z . The stellar temperature ranges between 10^4 K and $\geq 10^5$ K. A decreasing trend of T_* with increasing z can be noticed. Interestingly, the highest T_* are found in SB LINERs and the lowest ones in the starbursts calculated for optically faint ULRIGs at relatively high z . This indicates that the stars are younger in local galaxies. The stars formed in SB at higher z had the time to cool down. Some stars in the LINER sample galaxies which show SB characteristics, show temperatures of $\sim 10^5$ K, which are suitable to Wolf-Rayet stars. In fact they appear in the z range corresponding to higher than solar N/H. W-R stars were recently predicted in merger galaxies (Contini 2012a). The outstanding T_* in galaxies at $z \sim 2$ are discussed in Contini (2013, in preparation).

The flux from the AGN F (in units of 10^{10} photons $\text{cm}^{-2} \text{s}^{-1} \text{eV}^{-1}$ at the Lyman limit) and the ionization parameter U appear together in the diagram. The ionization parameter for LINERs is low, even lower than U calculated for compact galaxies (KZ99) at higher z . This could indicate that the flux is diluted by the large geometrical thickness D of the emitting clouds which can reach 1-10 pc in LINERs (Contini 1997). Alternatively, the radiation flux is obstructed on its way to the emitting clouds by patches of gas and/or dust. For the starbursts which could contribute to the AGN spectra observed by Ramos Almeida et al at higher z , U increases by a factor of ≤ 100 . We wonder how models calculated by these high U could fit eventually observed IR line ratios (cf Contini 2013a). Both F and U increase with z decreasing from $z=3.35$ to $z=0.5$. The shock velocity decreases in this range of z and the preshock density in SB clouds are low. Therefore the flux is less absorbed. Moreover, D has not yet reached the large thickness as those found for galaxies at $z \leq 0.1$.

Log F , which refers to AGNs in general, shows a rough maximum ($\log F \geq 11$) at $z \sim 0.1$, decreasing towards lower redshifts. The flux from the AGN in the Ramos Almeida et al (2013) (Paper I, table 3) and Brand et al. (Table

1) sample galaxies is moderately high ($F = 5.10^9 - 2 \cdot 10^{10}$ photon $\text{cm}^{-2} \text{s}^{-1} \text{eV}^{-1}$ at the Lyman limit)) similar to that characteristic of low-luminosity AGN, while it ranges within more than three orders of magnitude for the ensemble of the local AGNs.

3.3 Relative abundances

Fig. 3 left middle panel shows O/H, N/H, Ne/H and S/H (in 10^{-4} units) calculated consistently with the physical parameters by modelling the spectra. Unfortunately the spectra from Ramos Almeida et al (2013) reported in Paper I and those of Brand et al. (2007) do not contain data for the Ne and S lines.

The Ne/H relative abundances are solar and higher than solar (10^{-4} Allen 1976, $1.3 \cdot 10^{-4}$ Cunha et al 2006) up to $z \sim 0.1$ and slightly decrease at higher z . The S/H relative abundances are solar at low z . They slightly decrease up to $z \sim 0.4$ where they abruptly drop by a factor of ~ 10 for KZ99 star-forming HII regions. Sulphur can be easily trapped into dust grains. This trend is similar to that of N/H and O/H for KZ99 objects in agreement with KZ99 prediction that these objects are metal poor. The low metallicities in galaxies showing collision evidence are generally explained by acquisition of external gas in merging processes. However, the O/H and N/H dips characteristic of KZ99 objects at z between 0.1 and 0.5 seem connected to the characteristic low V_s of the sample. Lower than solar Mg/H and Si/H are also predicted for these objects. At shock velocities $\leq 100 \text{ km s}^{-1}$ collisional processes are less efficient, in particular, dust grain sputtering at the shockfront. Therefore O, N and S remain trapped into grains and molecules.

The N/H relative abundances for AGNs show fluctuations with a maximum almost twice solar at $z \leq 0.01$ and a minimum ≤ 0.5 solar at $z \sim 0.1$. In the starburst clouds N/H drops to lower than solar values by a factor ≤ 3 at $z \sim 0.1$. The decrease of N/H and O/H from solar to ~ 0.1 solar with z decreasing from 3.35 to 1 may indicate that at this redshift range dust and stars are forming, reaching their maximum rates at different z between $z \sim 1$ and $z \sim 0.16$.

O/H is nearly solar ($6.6 \cdot 10^{-4}$) for most of the galaxies. Guaita et al (2013) calculated for star-forming galaxies at $2 < z < 3 \log(O/H)+12 = 8.2-8.8$ (corresponding to $O/H=1.58 - 8.3 \cdot 10^{-4}$). The higher limit is in agreement with our results for the SBs in the optically faint ULIRGs by Brand et al (2007). The peculiar minimum of O/H and N/H ratios calculated in Paper I by AGN models for a few Ramos Almeida et al. objects, G53 and G107 at relatively high z , confirm that these galaxies are SB dominated rather than AGN, as predicted by their location in the BPT diagram (Fig. 1).

The scattering of the relative abundance results in the $0.1 \leq z \leq 1$. range is evident also for the physical conditions in nearly all the diagrams of Fig. 3, due to the different types of galaxies involved. In particular, the geometrical thickness of the emitting clouds increases by a factor > 10 towards local galaxies in agreement with lower shock velocities and a reduced fragmentation of matter.

The results presented in Fig. 3 show in general O/H higher than those calculated by the direct methods. This can be understood considering that using composite models the line intensities are calculated by the fractional abundance of the ion corresponding to the line, e.g. O^{++}/O for [OIII], (and by other factors such as the collisional strength and the statistical weight) which are integrated throughout the cloud recombination zone downstream. Here the electron temperature and density of the emitting gas are not constant but follow the gas cooling rate. The regions corresponding to low O^{++}/O are also accounted for. Namely, $[OIII]/H\beta \propto (\Sigma_i (O^{++}/O)_i / (H^+/H)_i) [O/H]$, where i refers to the slab downstream. The O/H relative abundance is adjusted in order to reproduce the observed line ratio. Using the direct method, the electron temperature is derived from the observed $[OIII]5007+/[OIII]4363$ and the electron density from $[OII]3727/[OII]3729$ (the $\lambda 3727$ and $\lambda 3729$ lines are generally blended). Then, the $[OIII]/H\beta$ line ratio is calculated adopting this temperature and this density and the O/H abundance is evaluated by fitting the observed line ratio.

3.4 $H\alpha$ absolute flux and the geometrical thickness of the emitting clouds

The middle right panel of Fig. 3 shows the trend of $H\alpha_{calc}$, the absolute $H\alpha$ flux calculated from the emitting clouds in the galaxy and the geometrical thickness of the emitting clouds D .

As already mentioned, D in both the SBs and the AGNs decreases strongly with increasing z from a maximum average of ≥ 1 pc to $\sim 10^{-3}$ pc. The clouds are more extended in SBs than in AGN NLR. The geometrical thickness of the clouds corresponding to the LINER sample were not specified for single objects presented by Contini (1997), nevertheless a 1 - 10 pc range is globally indicated, enhancing even more the decreasing trend of D with increasing z . The geometrical thickness of the emitting clouds ranges within three magnitude orders. A rather steep drop of D can be noticed for $0.1 \leq z < 1$.

$H\alpha_{calc}$, following the trend of the ionization radiation flux F along the redshift axis, shows a slightly increasing trend up to $z=0.1$ and a decreasing trend for $z \geq 0.3$ for

AGNs. The SBs show some discontinuity, as already mentioned.

The fluctuations for $0.1 < z < 0.5$ of n_0 and V_s calculated for the KZ99 sample translate to fluctuations of $H\alpha_{calc}$, because $H\alpha_{calc} \propto n^2$.

3.5 The radius of the NLR and of the SB surrounding clouds

The $H\alpha$ luminosities were collected from the literature or calculated by the observed $H\alpha$ fluxes $L_{H\alpha} = 4 \pi H\alpha d^2$, where $H\alpha$ is the reddening corrected observed $H\alpha$ fluxes at Earth and d the distance of the galaxies from Earth (calculated by the redshift, adopting $H_0=73 \text{ km s}^{-1} \text{ Mpc}^{-1}$).

The radius R of the emitting regions (the NLR for AGNs and the emitting regions surrounding the SB) is calculated by $L_{H\alpha} = 4 \pi H\alpha_{calc} R^2$ assuming uniform conditions. $H\alpha_{calc}$ is calculated at the emitting gas nebula by the $H\beta$ absolute flux which appears in Tables 2, 3, 4, 7, 11 and 12 for each model. $L_{H\alpha}$ and R are shown in the bottom left panel of Fig. 3.

Comparing the range of D with the range of R , a factor of $\sim 10^2 - 10^3$ is found, indicating that many clouds are located in the NLR and in the SB surroundings up to a maximum distance from the AGN and from the stars, respectively, given by R . Fig. 3 shows that R results are scattered throughout more than two orders of magnitude for $0.3 < z < 1$.

Concluding, considering the AGN feedback-driven star formation process (Ishibashi et al 2013), we have investigated the contribution of SBs and AGN to the galaxy spectra. We have found star temperatures $T_* \sim 4 \cdot 10^4$ K at relatively low z . The temperature of the stars decrease the higher the redshift, but a decreasing U and an increasing R hardly confirm compactness of galaxies at higher z . After some metallicity modulations in terms of higher than solar N/H at lower z and scattering of O/H between solar and 0.2 solar at $0.1 < z < 1$, the metallicities regain the solar values at $z \sim 3$. The $H\alpha_{calc}$ absolute fluxes emitted by the SB clouds follow the trend of the ionization parameter and of the stellar temperature, while for AGN $H\alpha_{calc}$ follows in particular the density trend.

3.6 Star formation rates

We now consider the SFR trend both for AGN and SB galaxies along the redshift axis. Generally the SFR is calculated by the luminosities in the near UV for high z galaxies and in the FIR when the data in the IR are available. Actually, we have not enough data to calculate L_{IR} for each object of our sample, but we can evaluate the $H\alpha$ luminosity.

The efficiency in forming stars is due to the number of photons reaching the gas and dust clouds from the photoionizing source and to compression by the shock in the emission line zone throughout the galaxy, i.e. the NLR in AGNs and the regions surrounding the SB.

Fig. 3 bottom left panel indicates that $L_{H\alpha}$ increases with z . If the ionizing radiation comes from stars with mass $M > 10^{10} M_\odot$, $SFR(M_\odot \text{ yr}^{-1}) = 7.9 \cdot 10^{-42} L_{H\alpha} (\text{erg s}^{-1})$. So the SFR decreased slowly from $> 100 M_\odot \text{ yr}^{-1}$ at $z > 1.15$ for AGNs to $\leq 0.001 M_\odot \text{ yr}^{-1}$ for low luminosity LINERs at $z \leq 0.001$, with a roughly smooth trend.

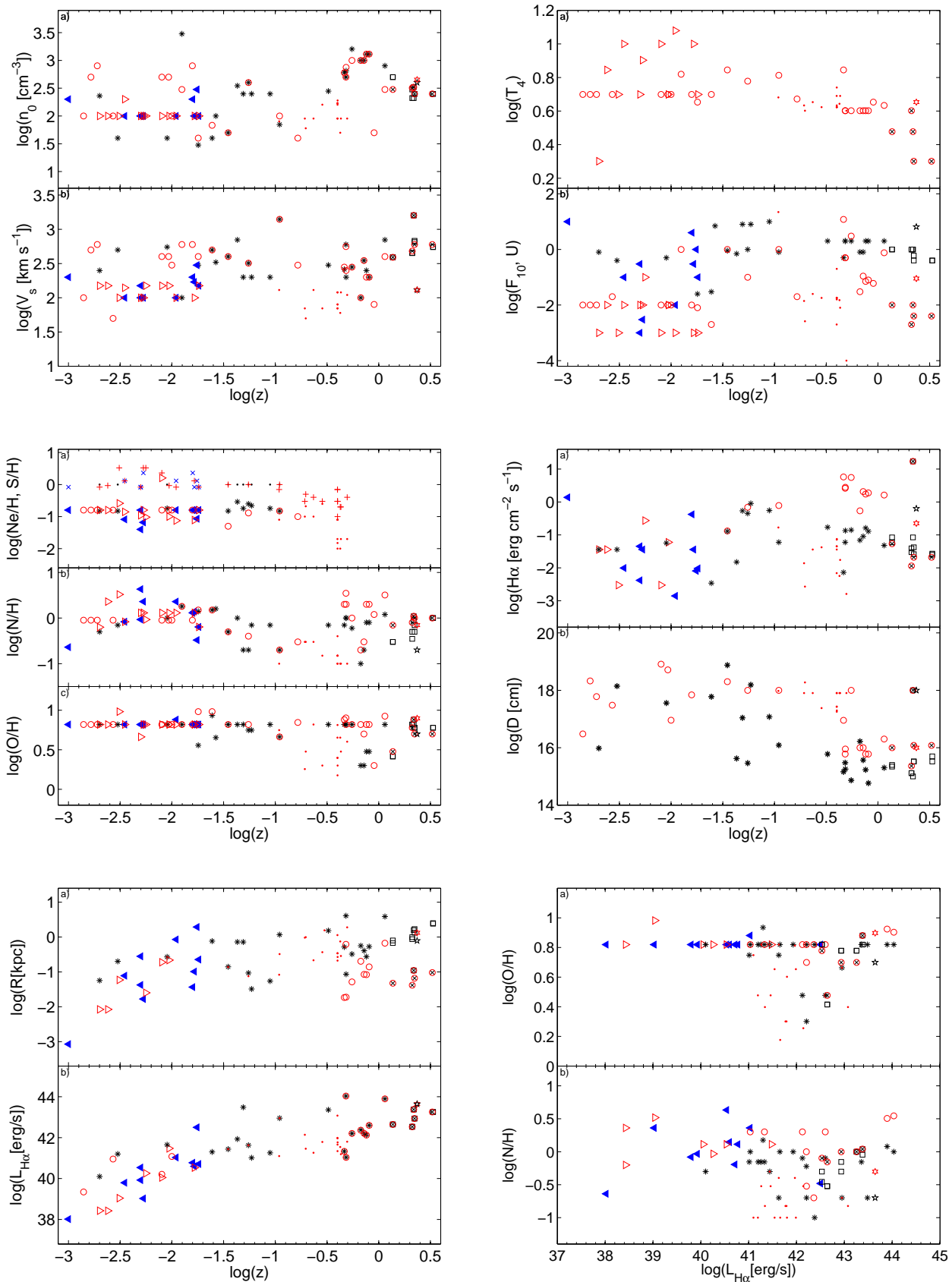


Figure 3. In all the diagrams red circles represent SB galaxies, red circles enclosing a x refer to the SBs in the optically faint ULIRGs; red triangles SB galaxies in the LINER sample, red dots the KZ99 galaxies, red hexagram ULIRGs; black asterisks the AGNs, black squares refer to the optically faint ULIRGs and blue filled triangles the AGNs belonging to the LINER sample; black pentagram ULIRGs. For Ne/H : red plus : starbursts; blue cross : LINER AGN ; black dots : AGN. Top left : n_0 and V_s ; top right : the radiation parameters T_4 and $F_{10, U}$; middle left : the abundances of Ne, N and O (in units of 10^{-14} phot $\text{cm}^{-2} \text{s}^{-1} \text{eV}^{-1}$ at the Lyman limit), the ionization parameter U and the temperature of the stars (in units of

The metallicity - redshift relation for massive stars is discussed by Pilyugin et al (2013) considering the various methods adopted to determine the O/H ratios from the spectral lines. They suggest that there is no correlation between oxygen abundance and specific star formation rates in massive galaxies. Neglecting the SFR - mass relationship (see e.g. Mannucci et al 2010) we present in Fig. 3 bottom right panel $\log(N/H)$ and $\log(O/H)$ versus $\log(L_{H\alpha})$ for a small number of galaxies, compared to the sample adopted by Pilyugin et al (2013 and references therein). Our results show that metallicity (in terms of O/H) correlates with $L_{H\alpha}$ (and therefore with SFR) particularly for SB galaxies with $L_{H\alpha} \geq 10^{41}$ erg s⁻¹. A rough correlation is seen also for N/H in the same range of $L_{H\alpha}$ with a large scattering due to the different types of galaxies. There seems to be no correlation for AGN and for low luminosity SB galaxies because O/H is roughly constant at the solar value. The critical redshift is $\sim 0.1 \leq z \leq 1$.

4 CONCLUDING REMARKS

We have modelled an heterogeneous sample of AGN and SB spectra observed at intermediate-high and low redshifts, in order to explore the evolutionary trend of some significant parameters. The sample is relatively poor in number of objects, but each of them has been analysed in details.

Our investigation started by modelling the spectra presented by Ramos Almeida et al (2013) for galaxies at intermediate redshift ($0.27 \leq z \leq 1.28$) in Paper I and ULIRGs at z between 1.37 and 3.35. Then we compared their physical conditions with those of galaxies at lower and higher z . Our approach was the following. After selecting the observed spectra containing enough number of lines to avoid degeneracy, the models were constrained by the comparison of calculated with observed line ratios. We adopted composite models which account consistently for the flux from a radiation source, outside the emitting clouds, combined with the shocks accompanying the gaseous cloud motion.

At relatively high redshift, the data become rare. The results show (Fig. 3) the evolution of physical conditions and the relative abundances in the gas within the galaxy sample on a large z range. The parameter trends are relatively smooth but their slopes change at different redshifts. This indicates that various process rates, such as e.g. star birth, relaxation from compact to diluted gaseous clouds, etc. have different rythms.

Summarizing, the evolution picture between $z=3.35$ and $z=0.001$ which results from our calculations shows that: 1) the gas in the emitting clouds of both AGNs and SB galaxies had a density broad peak at $z \sim 0.5$, becoming less dense and more elongated with time. 2) The flux from the AGN had a maximum at $z \sim 0.1$. 3) The star temperatures in SBs increased with time, indicating younger stars in local galaxies. 4) The O/H relative abundances split into various branches : from solar to 1/3 solar from $z=3.35$ to $z=0.6$. N/H shows a modulated trend. 5) The NLR of AGNs and the starburst surrounding regions were more fragmented at $z \geq 0.35$ due to higher shock velocities. 6) Metallicity (in terms of O/H) correlates with $L_{H\alpha}$ (and therefore with SFR) for massive galaxies with different trends for SBs and AGNs for

$L_{H\alpha} \geq 10^{41}$ erg/s. A rough correlation is seen also for N/H. There seems to be no correlation for low luminosity galaxies.

REFERENCES

- Allen, C.W. 1976 *Astrophysical Quantities*, London: Athlone (3rd edition)
- Anders E., Grevesse N. 1989, *Geochim. Cosmochim. Acta*, 53, 197
- Baldwin J. A., Phillips M. M., Terlevich R. *PASP*, 1981, 93, 5
- Brand, K., et al. 2007, *ApJ*, 663, 204
- Brinchmann, J., Charlot, S., White, S.D.M., Tremonti, C., Kauffmann, G., Heckman, T., Bronkman, J. 2004, *MNRAS*, 351, 1151
- Capetti, A., Robinson, A., Baldi, R. D., Buttiglione, S., Axon, D.J., Celotti, A., Chiaberge, M. 2013arXiv1301.5757C
- Caputi, K. et al. 2007, *ApJ*, 660, 97
- Cardelli, J.A., Clayton, G.C., Mathis, J.S. 1989, *ApJ*, 345, 245
- Chung, J., Rey, S.-C., Sung, E.-C., Yeom, B.-S., Humphrey, A., Yi, W., Hyeong, J. 2013 *ApJ*, 767, L15
- Contini, M. 2013a, *MNRAS*, 429, 242
- Contini, M. 2013b, *A&A*, submitted
- Contini, M. 2013c, *MNRAS*, arXiv1310.3619 (Paper I)
- Contini, M. 2012a, *MNRAS*, 426, 719
- Contini, M. 2012b, *MNRAS*, 425, 120
- Contini, M. 2009, *MNRAS*, 399, 1175
- Contini, M. 1997, *A&A*, 323, 71
- Contini, M., Aldrovandi, S.M. 1983, *A&A*, 127, 15
- Contini, M., Contini, T. 2003, *MNRAS*, 342, 299
- Contini, M., Cracco, V., Ciroi, S., La Mura, G. 2012, *A&A*, 545, 72
- Contini, M., Viegas, S.M., Prieto, M.A. 2002, *A&A*, 399, 414
- Cunha, K., Hubeny, I., Lanz, T. 2006, *ApJ*, 647, L143
- Diaz A. I., Prieto M. A., Wamsteker W., 1988, *A&A*, 195, 53
- Edmunds, M.G. & Pagel, B.E.J. 1978 *MNRAS*, 185, 77
- Fabbiano, G.; Wang, Junfeng; Elvis, M.; Risaliti, G. 2011, *Natur*, 477, 431
- Fosbury R. A. E., Wall J. V., 1979, *MNRAS*, 189, 79
- Fried, J. W.; Schulz, H. 1983, *A&A*, 118, 166
- Guaita, L., Francke, H., Gawiser, E., Bauer, F.E., Hayes, M., Östlin, G., Padilla, N. 2013, arXiv:1301.5600
- Gunawardhana, M.L.P. et al. 2013arXiv1305.5308G 2011, *A&A*, 529, 149
- Ho, L.C., Filippenko, A.V., Sargent, W.L.W. 1993, *ApJ*, 417, 63
- Hodapp, K.W., et al. 2003, *PASP*, 115, 1388
- Ishibashi, W., Fabian, A.C., Canning, R.E. 2013, arXiv:1302.4998
- Izotov, Y. I.; Stasiska, G.; Meynet, G.; Guseva, N. G.; Thuan, T. X. 2006, *A&A*, 448, 955
- Izotov, Y. I.; Guseva, N. G.; Fricke, K. J.; Stasiska, G.; Henkel, C.; Papaderos, P. 2010, *A&A*, 517, 90
- Izotov, Y.I., Guzeva, N.G., Thuan, T.X. 2011, *ApJ*, 728, 161
- Jannuzi, B.T., Dey, A. 1999, in *ASP Conf Ser.191, Photometric Redshifts and the Detection of High Redshift*

- Galaxies, ed. R.Weymann et al (San Francisco: ADP), 111
- Kauffmann, G. et al. 2003, MNRAS, 346, 1055
- Kakazu, Y., Cowie, L.L., Hu, E.M. 2007, ApJ, 668, 853
- Kewley, L.J., Dopita, M.A., Sutherland, R.S., Heisler, C.A., Trevena, J. 2001, ApJ, 556, 121
- Kobulnicky, H., Zaritsky, D. 1999, ApJ, 511, 118
- Krogager, J-K. et al. 2013, arXiv:1304.4231
- Madau, P., Ferguson, H.C., Dickinson, M.E., Giovalisco, M., Steidel, C.C., Fruchter, A. 1996, MNRAS, 283, 1388
- Mannucci, F., Cresci, G., Maiolino, R., Marconi, A., Gnerucci, A., 2010, MNRAS, 408, 2115
- McLean, I.S. et al. 1998, Proc. SPIE, 3354,566
- Osterbrock, D.E. Astrophysics of Gaseous Nebulae and Active Galactic Nuclei. Mill Valley, CA: University Science Books; 1989.
- Pagel, B.E.J., Simonson, E.A., Terlevich, R.J., Edmunds, M.G. 1992, MNRAS, 255, 325
- Pilyugin, L.S. et al. 2013, MNRAS, 432, 121
- Pustilnik, S.; Kniazev, A.; Pramskij, A.; Izotov, Y.; Foltz, C.; Brosch, N.; Martin, J.-M.; Ugryumov, A. 2004, A&A, 419, 469
- Ramos Almeida, C., Rodríguez Espinosa, J.M., Acosta-Pulido, J.A. Alonso-Herrero, A., Pérez García, A.M, Rodríguez-Eugenio, N. 2013, MNRAS, 429, 3449
- Santini, P. et al. 2012, A&A, 540, 39
- Schirmer, M., Diaz, R., Holhjem, K., Levenson, N.A., Winge, C. 2013, ApJ, 763, 60
- Seaton, M.J. 1975, MNRAS, 170, 475
- Shim, H., Colbert, J., Teplitz, H., Henry, A., Malkan, M., McCarthy, P., Yan, L. 2009, ApJ, 696, t85
- Spaans, M. & Carollo, C.M. 1997 ApJ, 482, L93
- Springel, V., Di Matteo T., Hernsquist, L. 2005, ApJ, 620, L79
- Swinbank, A.M., Smail, I., Sobral, D., Theuns, T., Best, P.N., Geach, J.E. ApJ, 2012, 760, 130)
- Stierwalt, S. et al 2013, ApJS, 206, 1
- Straughn, A.N. et al. 2009, 138, 1022
- Teplitz, H.I., Collins, N.R., Gardner, J.P., Hill, R.S., Rhodes, J 2003, ApJ, 589, 704
- Torres-Peimbert, S., Peimbert, M., Fierro, J. 1989, ApJ, 345, 186
- Veilleux, S., Kim, D.-C., Sanders, D.B. 1999 ApJ, 522, 113
- Viegas, S.M., Contini, M., Contini, T. 1999, A&A, 347, 112
- Vila Costas, M.B., Edmunds, M.G. 1993, MNRAS, 265, 199
- Winter, L.M., Lewis, K.T., Koss, M., Veilleux, S., Keeney, B., Muschotzky, R. 2010, ApJ, 710, 503
- Xia, L. et al. 2012, AJ, 144, 28